

Cross-field chaotic transport of electrons by $\mathbf{E} \times \mathbf{B}$ electron drift instability in Hall thrusters

D. Mandal^{1,2}, Y. Elskens¹, N. Lemoine³ and F. Doveil¹

¹ Aix-Marseille Université, CNRS, UMR 7345-PIIM Laboratory, Marseille, France

² Indo-French Centre for the Promotion of Advanced Research-CEFIPRA, New Delhi, India

³ Université de Lorraine, Institut Jean Lamour, UMR-7198, CNRS, France

Abstract

One special interest for the industrial development of Hall thruster is characterizing the anomalous cross-field electron transport observed after the channel exit. Since the ionization efficiency is more than 90%, the neutral atom density in that domain is so low that the electron collisions cannot explain the high electron flux observed experimentally. Indeed this is 100 times higher than the collisional transport. In Hall thruster geometry, as ions are not magnetized the electric and magnetic field configuration creates a huge difference in drift velocity between electrons and ions, which generates electron cyclotron drift instability or $\vec{E} \times \vec{B}$ electron drift instability. Here we are focusing on collision-less chaotic transport of electrons by those unstable modes generated by $\vec{E} \times \vec{B}$ drift instability. We found that in presence of these electrostatic modes electron dynamics become chaotic. They gain energy from the background waves which increases electron temperature along perpendicular direction by a significant amount, $T_{\perp}/T_{\parallel} \sim 4$, and a significant amount of crossfield electron transport is observed along the axial direction.

Introduction and numerical model

In Hall thruster geometry, the electric and magnetic field configuration creates a huge difference in drift velocity between electrons and ions, which generates electron cyclotron drift instability or $\vec{E} \times \vec{B}$ electron drift instability [1]. Unstable modes generated from this instability have an important role in cross-field anomalous transport of electrons. One special interest for the industrial development of Hall thruster is characterizing the anomalous cross-field electron transport observed after the channel exit. Since the ionization efficiency is more than 90%, the neutral atom density in that domain is so low that the electron collisions cannot explain the high electron flux observed experimentally. Here we focus on collision-less chaotic transport of electrons by the unstable modes generated by the $\vec{E} \times \vec{B}$ drift instability. These unstable modes can evolve at a sufficient level of turbulence into a non-magnetic ion-acoustic instability with modified angular frequency given [2] by,

$$1 + k^2 \lambda_{De}^2 + g \left(\frac{\omega - k_y v_d}{\omega_{ce}}, (k_x^2 + k_z^2) \rho_e^2, k_x^2 \rho_e^2 \right) - \frac{k^2 \lambda_{De} \omega_{pi}}{(\omega - k_z v_{i,b})^2} = 0, \quad (1)$$

where λ_{De} is the electron Debye length, $v_d = E_z/B$ is the electron drift velocity, $v_{i,b}$ is the ion beam velocity, $\rho_e = v_{the}/\omega_{ce}$ is the electron Larmor radius, v_{the} is the electron thermal velocity. We consider a Cartesian coordinate system, x -direction as magnetic field direction, y -direction as $\vec{E} \times \vec{B}$ drift direction and z -direction as constant electric field direction, which are the radial, azimuthal and axial direction of the thruster chamber, respectively. ω , ω_{ce} and ω_{pi} are the mode, electron cyclotron and ion plasma frequencies, respectively, and g is the Gordeev function [5]. This analytical model for the dispersion relation fits well with the experimental data. We consider a constant electric field $E_0 \hat{z}$ along the z -direction and a constant magnetic field $\vec{B} = B_0 \hat{x}$ along x -direction.

Experimentally, the observed propagation angle of the instability-generated wave deviates by $\tan^{-1}(k_z/k_y) \sim 10 - 15^\circ$ from the azimuthal y -direction near the thruster exit plane. Further from the exit plane, the propagation becomes progressively more azimuthal [1]. Hence, the wave vector along axial direction $k_z \sim 0.2k_y$, and the electric field along the axial direction is dominated by the stronger constant field $E_0 \hat{z}$. Therefore for simplicity, we consider that the unstable modes are confined in $x - y$ (ie., $r - \theta$) plane only. Then the time varying part of the potential in $x - y$ plane is constructed

as a sum of unstable modes. The total electric field acting on the particle is

$$\vec{E}(x, y, z, t) = \sum_n \phi_{0n} [k_{nx} \sin \alpha_n(x, y, t) \hat{x} + k_{ny} \sin \alpha_n(x, y, t) \hat{y}] + E_0 \hat{z}, \quad (2)$$

with the phase $\alpha_n(x, y, t) = k_{nx}x + k_{ny}y - \omega_n t + \zeta_n$, where n is a label for different modes with wave vector \vec{k}_n , angular frequency ω_n and phase ζ_n . \vec{k}_n , ω_n follow the dispersion relation eq. (1) and phases ζ_n are random. Here the position \vec{x} , velocity \vec{v} , time t and the potential ϕ_0 are normalized with Debye length λ_{De} , thermal velocity v_{the} , electron plasma frequency ω_{pe}^{-1} and $m_e v_{the}^2 / q$, respectively. We choose the amplitude ϕ_{0n} of all the modes equal to the saturation potential at the exit plane of the thruster $|\delta\phi_{y,rms}| = T_e / (6\sqrt{2}) = 0.056 v_{the}^2$ [3]. We consider three modes ($n = 1, 2, 3$) with $(k_{nx}, k_{ny}, \omega_n) = (0.03, 0.75, 1.23 \times 10^{-3})$, $(0.03, 1.5, 1.7 \times 10^{-3})$ and $(0.03, 2.25, 1.87 \times 10^{-3})$, respectively. In normalized units, $qB_0/m_e = 0.1\omega_{pe}$, $qE_0/m_e = 0.04\omega_{pe}v_{the}$, and $v_d = 0.4v_{the}$. The equations of motion of the particle are

$$\frac{d\vec{x}}{dt} = \vec{v}, \quad \frac{d\vec{v}}{dt} = \vec{E} + \vec{v} \times \vec{B}. \quad (3)$$

Because \vec{E} depends on space, the infinitesimal generators for both equations do not commute, and one uses a time-splitting numerical integration scheme. The first equation is integrated in the form $\vec{x}(t + \Delta t) = \mathcal{T}_{v,\Delta t}(\vec{x}(t)) = \vec{x}(t) + \vec{v}\Delta t$. For the second equation, we separate the electric integration $\vec{v}(t + \Delta t) = \mathcal{T}_{E,\Delta t}(\vec{v}(t)) = \vec{v}(t) + (q/m)\vec{E}\Delta t$ from the magnetic integration, which solves only the gyro-motion. For the latter, we use the Boris method [4], formally $\vec{v}(t + \Delta t) = \mathcal{T}_{B,\Delta t}\vec{v}(t)$. As a result, we use a second-order symmetric scheme

$$\begin{pmatrix} x(t + \Delta t) \\ y(t + \Delta t) \end{pmatrix} = \mathcal{T}_{v,\Delta t/2} \circ \mathcal{T}_{E,\Delta t/2} \circ \mathcal{T}_{B,\Delta t} \circ \mathcal{T}_{E,\Delta t/2} \circ \mathcal{T}_{v,\Delta t/2} \begin{pmatrix} x(t) \\ y(t) \end{pmatrix}.$$

Time evolution of particle trajectory and velocity

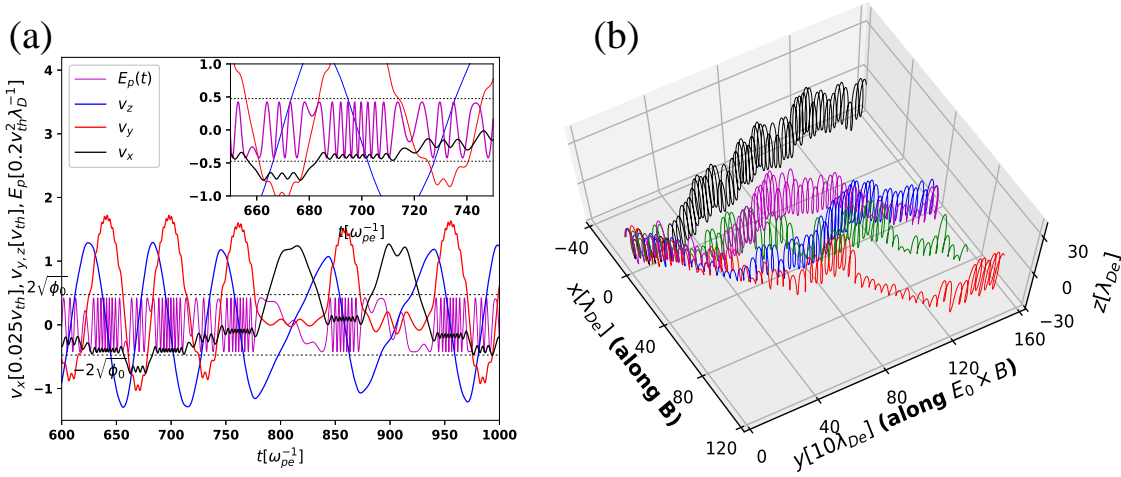


Figure 1: Particles evolution in the presence of a single background electrostatic wave with $n = 2$. Panel (a): velocity components v_x (black solid line), v_y (red) and v_z (blue) of one particle. Magenta line: electric field at particle location. Near $t = 800$ and 900 , the particle is trapped in the wave potential and it oscillates with the time period $\tau_b = 18\omega_{pe}^{-1}$. Panel (b): trajectories of 5 different particles with different initial phase.

We solve the equation of motion Eq. (3) numerically for 1056 particles. In the absence of the background electrostatic waves $E_x = E_y = 0$, their trajectories are regular and exhibit cyclotron motion with a drift velocity $v_d = 0.4$. Therefore, their velocity components are $v_x = v_{0x}$, $v_y = v_{\perp 0} \cos(\omega_c t) + v_d$ and $v_z = v_{\perp 0} \sin(\omega_c t)$, where $v_{\perp 0} = \sqrt{v_{0z}^2 + (v_{0y} - v_d)^2}$ and (v_{0x}, v_{0y}, v_{0z}) are the initial velocity components. In the presence of the background electrostatic wave, the wave-particle interaction modifies their cyclotron motion. The strength of the wave-particle interaction depends on the wave amplitude

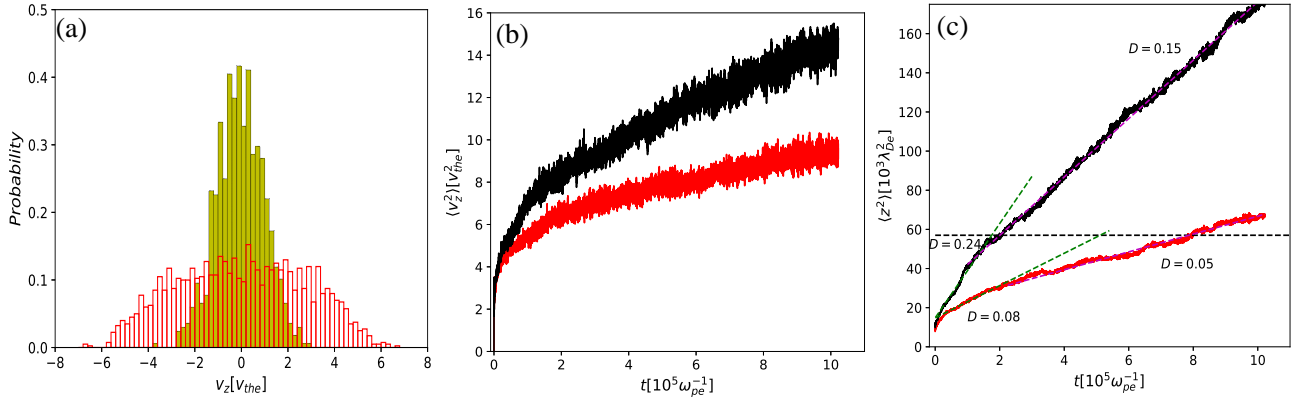


Figure 2: Panel(a): initial (yellow solid bar) and final (bar with red boundary) velocity distribution along z at $t = 5 \times 10^4 \omega_c^{-1}$. Panels (b) and (c): mean square velocity dispersion $\langle v_z^2(t) \rangle$ and mean square displacement $\langle z^2(t) \rangle$, respectively. The red and black lines correspond to no-boundary and reflecting boundary cases, respectively. Panel (c) reveals two diffusion regimes in each curve, namely (0.08, 0.05) for no-boundary and (0.24, 0.15) for reflecting boundary.

and the particle velocity. Fig. 1(a) presents the time evolution of the three velocity components and the electric field $E_p(t)$ (magenta line) at the particle location. Due to the cyclotron motion, v_y oscillates about the drift velocity v_d (solid red line). During each cyclotron oscillations, when $|v_y| \leq 2\sqrt{\phi_0}$ (denoted by black dashed lines) the particle strongly interacts with the electrostatic wave, and the electric field $E_p(t)$ increases/decreases the v_x value by large amount. The inset of Fig. 1(a) presents, during strong interaction, according to the sign of E_p , jumps of v_x (black solid line) in positive and negative direction. Moreover, during this strong interaction depending on the local potential profile, the particle may be trapped in the wave potential well and oscillate with the bounce-frequency $\omega_b = 0.35\omega_{pe}$. In Fig. 1(a) near $t = 800$ and 900 , it is trapped. One essential condition for the trapping is $\omega_b > \omega_c$, where $\omega_b = k_y \sqrt{q\phi_0/m}$ is the bounce frequency. Since $k_y \gg k_x$, the condition for trapping is easily satisfied along the y -direction, therefore the particle bounces back and forth along y -direction and moves freely along the x -direction. Hence along x -direction it gains/loses energy from/to the wave which causes a large change in v_x . Finally, depending of the local potential value, it may escape from the wave and again start to exhibit cyclotron motion. Therefore the duration of trapping depends on v_x and ω_b/ω_c . It is observed that, for small $v_x \ll \sqrt{\phi_0}$, this trapping is easily observed for $\omega_b/\omega_c \geq 2$. Outside the strong interaction region, due to the large particle velocity, electric field at particle location E_p changes rapidly, which generates the small-amplitude fast oscillation in v_x . v_y is also modulated due to this fast change in $E_p(t)$. Since the electric field along z -direction $E_0 \hat{z}$ is constant, the amplitude of the fast oscillation in v_z is negligible. The motion along z -direction is coupled with the other two directions due to $\vec{v} \times \vec{B}$ term of Lorentz force, therefore v_z is also modified during the strong interactions. In fig. 1(a) at $t = 900$, during trapping, the oscillation of v_z is observed with frequency ω_b , on top of cyclotron motion.

Fig. 1(b) presents the trajectories of 5 particles with slightly different initial phases. In the absence of the electrostatic wave, they exhibit cyclotron motion with drifting guiding center, and their trajectories remain confined in $y-z$ plane. Due to the strong interaction with the electrostatic wave in presence of magnetic field, each trajectory evolves differently and separates exponentially from each other, and the dynamics become chaotic. During each strong interaction, there is a change in the trajectories along x , and during trapping their average y location remain unchanged. The duration of strong interaction depends ω_b/ω_c , therefore for single wave chaos will occurs for amplitude ϕ_0 satisfy $\phi_0 > \omega_c^2/k_y^2$. For thruster parameter values, all three waves satisfy this criterion. In the presence of two and three waves, the dynamics become more chaotic and this threshold value is reduced.

Energy gain by the particles and their axial transport

To analyze transport, we consider 1056 particles with random initial positions in the rectangle $0 \leq y_0 \leq 4\pi/k_{1y}$, $0 \leq x_0 \leq 2\pi/k_{1x}$ and with velocities drawn from a 3D Gaussian distribution with unit standard-deviation along all three directions. Then we evolve their dynamics in presence of all three waves with equal amplitude $\phi_{n0} = \phi_{0,\text{rms}}$. For single wave interaction, the Hamiltonian of the dynamics can be written in a time independent form and therefore, though the dynamics remain chaotic, there is no net gain/loss of energy over long time evolution. But in presence of two/three waves, the Hamiltonian is no more time independent, all the trajectories become chaotic and due to the wave particle interaction they gain energy from the waves. Their net perpendicular velocity v_y, v_z increase. After sufficiently long time-evolution, they form a Gaussian-like velocity distribution profile with higher temperature along y - and z -directions. Since $E_x \ll E_{y,z}$, the increase of the velocity component along the magnetic field is negligible compared to the other two directions. Therefore the temperature along the magnetic field remains nearly unchanged. Fig. 2(a) presents the initial ($t = 0$) (solid yellow bars) and final ($t = 5 \times 10^4 \omega_c^{-1}$) (bars with red border) velocity distribution of v_z , which presents a significant increase of temperature along perpendicular direction T_\perp compared to the parallel direction, $T_\perp/T_\parallel \sim 4$.

In the thruster chamber, there is an insulating boundary along x -direction. The width of the annular space in the thruster is $240\lambda_{De}$. Therefore the particles are reflected when they reach to the boundary. If there were no reflection, particles would proceed under the same dynamics (red line in Fig. 2(b)-(c)). To account for reflection (black line), we consider the Debye sheath electron potential energy near the wall to be $\phi_{sh} = 20\text{eV} = 0.8v_{the}^2$. Electrons reaching the wall with $v_x < \sqrt{0.8}$ are specularly reflected, and electrons with $v_x > \sqrt{0.8}$ are isotropically reflected from the wall with conserving their total energy. Fig. 2(b)-(c) present $\langle v_z^2(t) \rangle$ and $\langle z^2(t) \rangle$ for reflecting boundary (black) and without boundary (red), where $\langle \rangle$ denotes the average over number of particles. The duration of strong interaction with the waves and hence the gain of energy from the waves decrease with increase of particle velocity. Therefore, the rate of energy gain in Fig. 2(b) decreases with time for both cases. In isotropic reflection, the velocity components of the particle are redistributed randomly in three directions, a particle with small v_y and v_x gains more energy from the electrostatic wave compared to that having higher v_y and v_x . Therefore, in presence of reflecting boundary, particles gain more energy than in absence of reflection. The dashed black line marks the location of thruster outlet along the z -direction. Since with reflection they gain more energy, their mean square displacement along z -direction crosses the thruster outlet, and they exit from the thruster chamber more quickly than in the case without boundary. For both cases, we found two different diffusion coefficient ($D = d\langle z^2 \rangle/dt$), values, which are ($D = 0.08, 0.05$) for no-reflection and ($D = 0.24, 0.15$) for reflecting boundary. The change in slope around $t = 2 \times 10^5 \omega_{pe}^{-1}$ is related to the structure of the stochastic web controlling the velocity transport [6, 7].

Due to the chaotic dynamics, in presence of the single wave also we get a crossfield transport along z direction, but the diffusion coefficient is very small. As the electric field E_y is proportional to k_y , waves with different \vec{k} values induce different diffusion coefficients and energy gain rates.

Conclusions

Due to strong interaction with the wave potential, the drifted cyclotron motion becomes chaotic. In presence of more than one wave electrons gain energy over long time evolution and their temperature is increased. This chaotic dynamics helps in transport of electrons along the thruster axial direction. Significant amount of axial electron transport is observed in presence of more than one waves, and the electrons exit from the thruster chamber. The reflection at boundary enhances the transport coefficient.

Acknowledgements

This work is part of IFCPRA project 5204-3. We acknowledge the financial support from CEFIPRA/IFCPRA. We are thankful to the Aix-Marseille University MesoCentre for computations. We are grateful to Professors Xavier Leoncini, Dominique Escande and Abhijit Sen for many fruitful discussions and their comments.

References

- [1] S. Tsikata, C. Honoré, N. Lemoine, D. M. Grésillon, *Phys. Plasmas* **17**, 112110 (2010)
- [2] J. Cavalier, N. Lemoine, G. Bonhomme, S. Tsikata *et al.*, *Phys. Plasmas* **20**, 082107 (2013)
- [3] J. P. Boeuf and L. Garrigues, *Phys. Plasmas* **25**, 061204 (2018)
- [4] J. Boris, Proc. Fourth Conf. Numer. Simul. Plasmas, NRL, Washington, D.C., pp. 3-67, (1970)
- [5] G. V. Gordeev, *Zh. Eksp. Teor. Fiz.* **23**, 660 (1952) [*Sov. Phys.-JETP* **6**, 660 (1952)]
- [6] G. M. Zaslavsky, *Chaos* **1**, 1 (1991).
- [7] X. Leoncini *et al.*, *C. R. Mécanique* **336**, 530 (2008).